Chapter 7

BLOCK-CHAIN AND ITS IMPACT ON AGGREGATED LOAD PROFILE AND AVAILABLE DISTRIBUTION CAPABILITY

7.1 INTRODUCTION

Power grids monitoring, operation, control, and commercialization is transforming gradually due to the technological advancements, and new frontiers of distinct applications are emerging in this field. Global emphasis on increasing the dependence on renewable sources of generation, along with a focus on electric vehicles as a means of transportation, has the potentials of affecting the traditional notion of grid analysis, monitoring, and control. The prevalence of communicable intelligent devices enables peers to transact and sell/buy power locally or to the grid. Ensuring security, privacy, and avoidance of double-spending in these transactions could be manifested by utilizing the blockchain technologies' developments. In this chapter, IEEE 24 bus test distribution system has been considered. The effect of incorporating the energy transactions over block-chain in ADN on Available Distribution Capability, Aggregated load profile, and load-ability is evaluated. The effect has been quantified using $\boldsymbol{BC_{ef}}$ proposed in this article. It has been observed that enabling intelligent electronic devices and peers to a transaction over a blockchain can improve the performance of the ADN. The major contributions of this chapter are: -

- A new index (BC_{ef}) have been proposed for quantizing the effect considering the BC-based energy trading.
- The concept of localized marginal clearing price and localized marginal clearing volume for localized ADN under consideration have been proposed.

- The effect on considering the DER integration and blockbased energy trading on load-ability of the overall ADN under consideration is presented.

7.2 BLOCK-CHAIN TECHNOLOGY IMPLEMENTATION

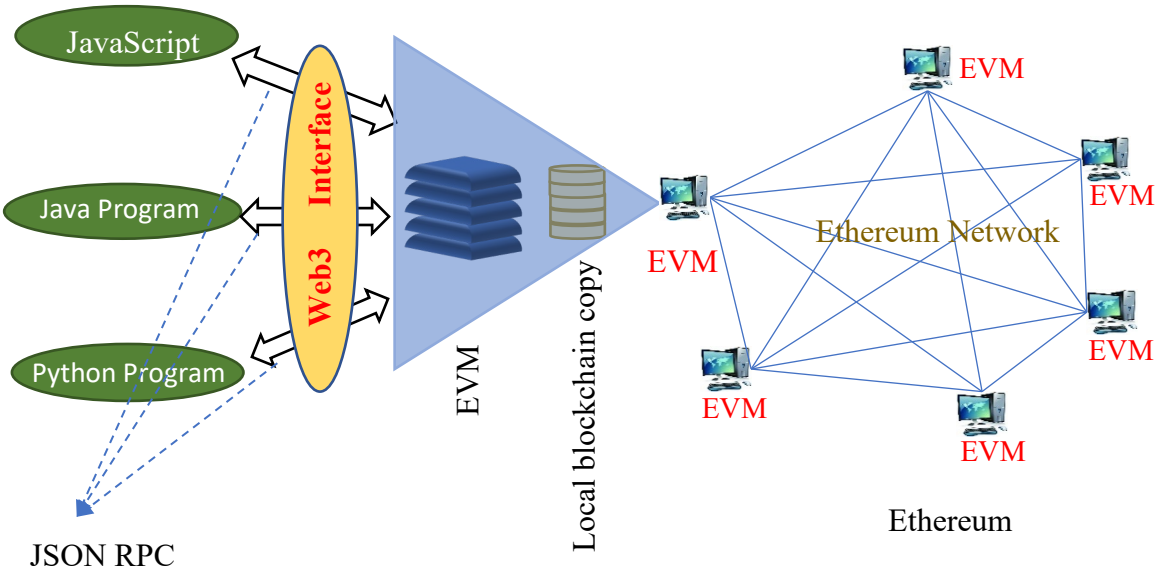

Figure 7.1 Schematic illustration of Blockchain implementation through the python interface.

The schematic representation of the ethereum based blockchain implementation has been illustrated in Figure 7.1. The smart contract deployed in blockchain could be accessed either from the front-end user applications (ethereum wallets), dedicated front end applications/web interfaces, or Web3 Interface for developmental purposes. Web3 interface could be exploited for accessing the smart contract deployed on the ethereum blockchain through the EVM (Ethereum Virtual Machine) node. The Web3 interface could be used either by Python, JavaScript, or Java Programme.

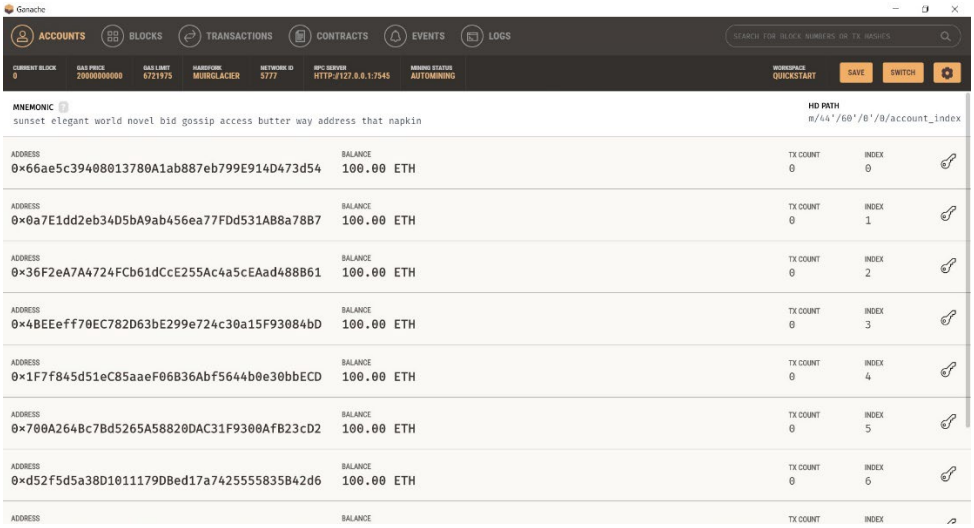

Figure 7.2 Ganache Interface

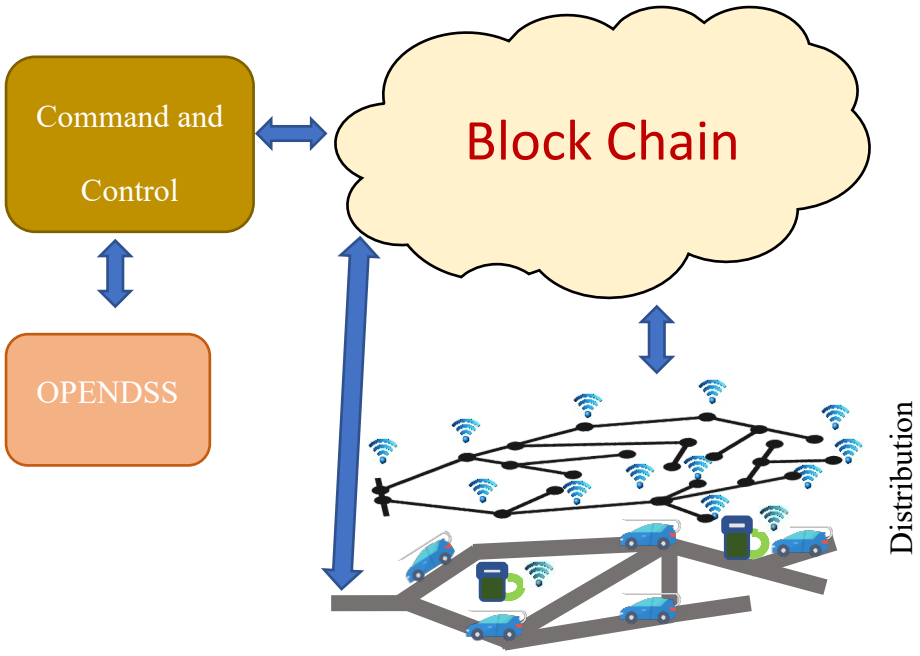

Figure 7.3 Schematic illustration of the interaction between various components of the smart grid.

For the work under consideration, we have used python language through the Web3.py library to access the blockchain deployed in the Ganache environment at the localhost of the system. The developmental process requires accessing the private and public keys of

multiple accounts (of blockchain environment). The transaction would cost money in terms of gas (blockchain unit for transaction charge); therefore, we have used the ganache simulation environment for the entire developmental process. In Figure 7.2, the Ganache environment is used for developing and testing ethereum based blockchain smart contracts. The smart contracts are created using Solidity. Solidity is a language used for creating smart contracts for ethereum blockchain.

The interaction between various components of the smart grid has been shown in Figure 7.3. The participants, namely the LA (Local Aggregators), EV owners, Electric Vehicle Charging Stations (EVCS), DER's, grid would exchange their bids to the blockchain. The information of settled transactions is acquired by the command and control center and communicated to the DSO. The DSO validates the transaction and obtains the optimal settings of the devices for the settled transaction.

7.3 TECHNO-ECONOMIC OPERATION OF *ADN* USING THE BLOCKCHAIN-BASED FRAMEWORK

The impact of changing technologies has been schematically illustrated in Figure 7.4, along with their features. Block-chain, preliminary introduced as a distributed ledger for recording and exchanging value by Satoshi Nakamoto [128]. Since then, applications of blockchain technology arose in varied dimensions. Block-chain comprises blocks that are nothing but a continuously growing list of data records. The blocks forming the blockchain are immutable, secure, and connected to the preceding block. Any peer can initiate transactions in the blockchain network. The blocks registering the transaction to the blockchain will be considered valid if accepted and approved by all the nodes in the network. The validation process for the blocks ensures their semantic and syntactic correctness. The transactions registered through the blocks on the block-chain could be accessed and verified by any node in the network. SHA256 [166] based hashing algorithm

has been utilized for ensuring the security of each block. The hash of $(i-1)^{th}$ block is imbibed as an input to SHA256 function for obtaining the hash to subsequent block (i^{th}). Such a hashing system ensures that tempering at any one block creates an invalid condition among all the subsequent blocks in the chain. A consensus algorithm, along with the amalgam of the features mentioned above, protects the blockchain against colluding nodes with a certain degree of security and makes it highly resilient to tampering.

A schematic illustration of the proposed blockchain-based framework is shown in Figure 7.5. The distributed coalition formation based permission blockchain framework has been used. At each time instant, the information of actual power drawn/injected to the grid is communicated to the blockchain along with the bid for the impending instant. For each instance, the (Localized Market Clearing Price and Localized Marginal Clearing Volume) is determined, and the information is sent to the DSO. In DSO, the transactions are validated (feasibility of each transaction is checked), and the settled price is updated and send back to the blockchain network. The peer network of the ADN comprises the following auctioneers.

- Electric Vehicle Charging Stations (EVCS) deployed at various nodes in the ADN.
- The distributed generations (DERs) presented in the ADN.
- The bids are submitted by the individual loads (considered as intelligent devices) through the LA (local aggregators).
- Transmission grid (selling or purchasing at the p.c.c. depending on the operating situations.)

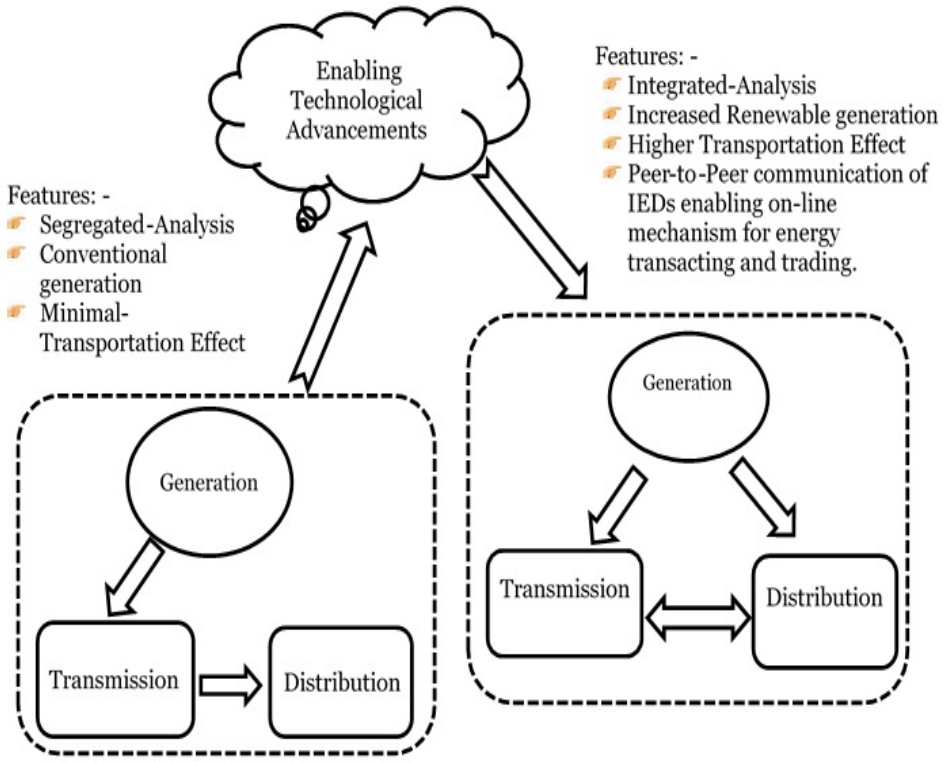

Figure 7.4 The changing technologies and their impact: - schematic representation.

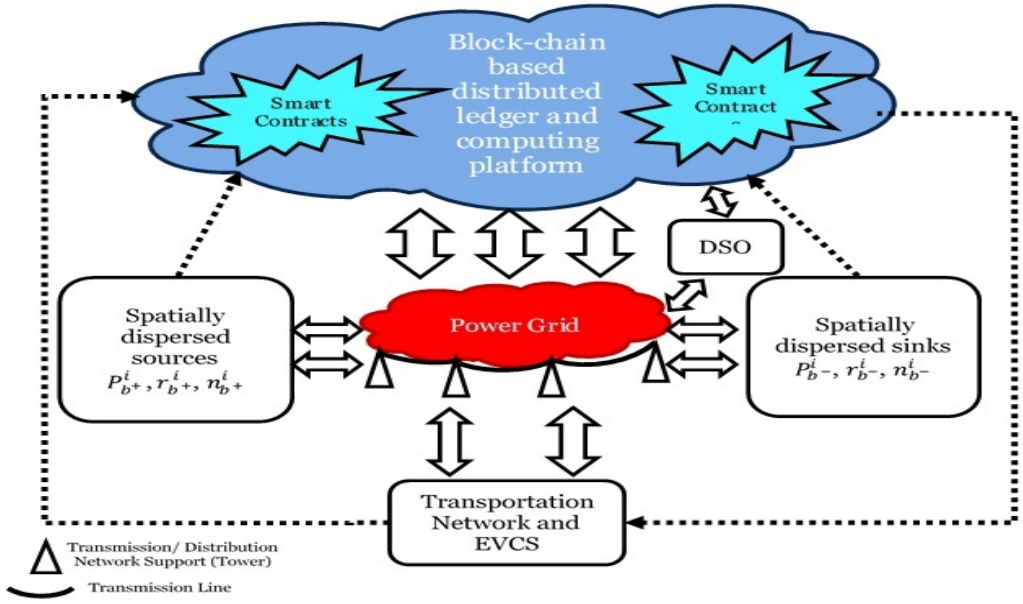

Figure 7.5 Schematic representation of blockchain implementation in ADN.

The flow chart for the energy scheduling and settlement process has been shown in Figure 7.6. The bid settlement process using the proportional sharing method has been discussed and given in [126]. In the PS method, the total demand and losses of the ADN are proportionally shared among the bidding generators by the block-chain. In this chapter, LMCP and LMCV based methods have been proposed for determining the settlement price. The procedure for LMCP and LMCV determination is given hereunder: -

7.3.1 LMCP and LMCV determination: -

The LMCP determination has been proposed under the following assumptions: -

a) The sellers and buyers participate in the bidding process through their bid functions $\mathcal{S}_i, \mathcal{B}_i$.

b) The sellers and buyers adhere to the following rules: -

i) The sellers and buyers will post their bids for the impending hour to the block chain based transacting energy framework.

ii) The sellers and buyers will post their actual consumption of the present hour to the block chain based transacting energy framework

Under these assumptions, a fair clearing price based mechanism has been proposed here and utilized in this article for determining the LMCP and LMCV of the considered ADN. Let,

$$\mathcal{S}_i\left(Pg_{i,t}\right) = \alpha_i \mathcal{IC}_i \times Pg_{i,t} + \mathcal{OM}_i \times Pg_{i,t} \quad 7.1$$

$$\mathcal{B}_i\left(Pd_{i,t}\right) = \beta_i Pd_{i,t}^2 + \psi Pd_{i,t} + \zeta_i \quad 7.2$$

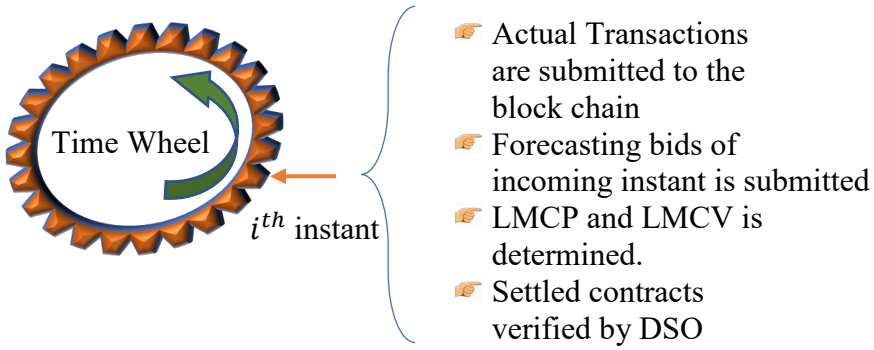

Figure 7.6 Sequential bid submission process on the block-chain.

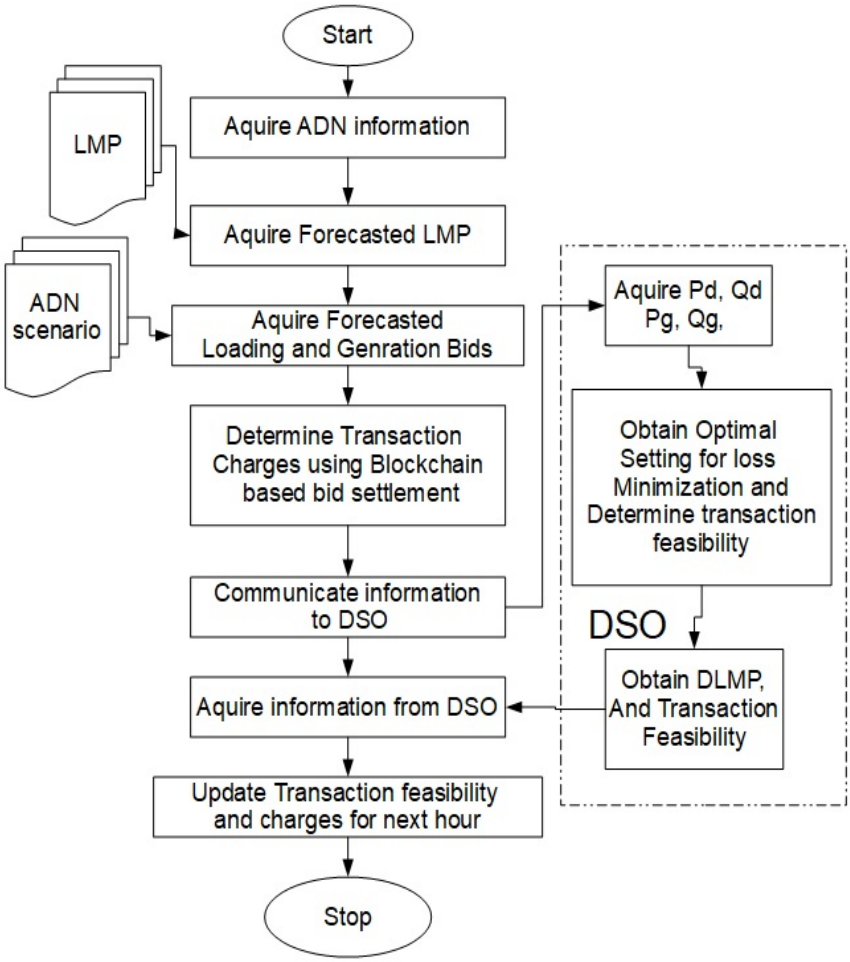

Figure 7.7 Flow chart for energy transaction scheduling and settlement process.

Here, α_i, is the cost of depreciation per unit, $\mathcal{IC}_i$ is installation cost per unit, $\mathcal{OM}_i$ operation and maintenance cost per unit of i^{th} bidding DER unit at time instant t, β_i, ψ_i and ζ_i are the bid function coefficient of the i^{th} bidding unit at time t. The sellers and

buyers determine their impending hour production/demand using adequate forecasting technique, use this for obtaining their bid price. These two values are posted to the blockchain-based framework. The process has been schematically illustrated in Figure 7.6. The steps of the LMCP and LMCV determination have been given in Table 7.1, and the overall process has been shown in Figure 7.7.

Table 7.1 Steps for obtaining the LMCP and LMCV

Steps	Algorithm
I	Acquire the bid prices from each local participant participants (including both buyers and seller, and Transmission grid bidding with LMP)
II	Arrange the sellers in increasing order of their bids and buyers in the decreasing order of their bids.
III	Find the point of intersection of the two curves (seller bid curve and buyer bid curve).
IV	The point of intersection would yield the LMCP and LMCV
V	If the grid is a seller and the LMCP determined is greater than the grid bid i.e., LMP set the LMCP to LMP
VI	Post the LMCV and LMCP to the DSO for validation of the transaction.

7.4 AVAILABLE DISTRIBUTION CAPABILITY, AGGREGATED LOAD PROFILE & LOADABILITY MARGIN

The net load profile subtended the interface of transmission level by the ADN can be defined as the Aggregated Load Profile (ALP). The ALP of the ADN would be depending on the participation of various energy vendors as well as active loads of ADN. Therefore, incorporating the energy transaction over the blockchain-based framework would also have a probable impact. Active load implies that the load would respond to price signals, provide bids for impending transactions, and send information pertaining to actual transactions to the block-chain through communicable intelligent devices. The total load profile represents the total load connected to the system; therefore, the ALP of an ADN would be different from its total load profile. ALP, in the simple sense, would be the total power injected/drawn at the TN (transmission network) interface. Thus, Aggregated Load of the ADN at time t would be obtained using the (7.3).

$$AL_t = \sum_{ns}^{i=1} P_{i,t}^{PSS_{Trf}} \qquad 7.3$$

In the above equation $P_{i,t}^{PSS_{Trf}}$ is the subtended load at the i^{th} source transformer of the ADN. The maximum additional load that could be served by the generating entities to the nodes in the ADN while providing for the existing distribution commitments while satisfying the constraints of distribution has been defined as available distribution capability. Analogous to ATC (Available transmission capability) at the transmission level, the ADC has been defined at the distribution level. ADC could be defined mathematically as (7.4).

$$ADC = DC - (EDC + DR) \qquad 7.4$$

In the above equation, TDC , EDC, and DR are the total distribution capability, existing distribution commitments, and distribution reserves. DR has been provided so that the DG's could handle the weather uncertainties. The load-ability margin at any operating state of the distribution system refers to the maximum load that can be served by the ADN under the allowable limits of voltage deviations while maintaining the other system constraints within limits.

$$\max(\mathcal{L}) \tag{7.5}$$

$$where, \mathcal{L} = \sum_{i} Pd_i \tag{7.6}$$

The optimization given above is solved while adhering to the impediments of the distribution power flow.

7.5 *ADN* COMPONENT MODELLING

7.5.1 Electric Vehicles and their Charging

The complete psychological and techno-economic and behavior pertaining to EV operation are modeled using an Agent-based approach. In Table 7.2, the taxonomy of the EV structure has been given, and Table 7.3 shows the charging station structure. The behavior of EV driving and charging has been modeled extensively by taking the number of vehicles as $N_{vehicle}$ and using β distribution function for representing the transportation network load and traffic. It is assumed that the EV are publicly owned by the State Transport Corporation. The net power drawn or injected by the EV can be obtained as

$$E^{\{EV,i\}} = P_{\{t\}}^{\{EV,i\}} \times (t_{start} - t_{stop}) \tag{7.7}$$

$$P_t^{\{EV,i\}} = \begin{cases} c_t^{\{r,i\}} & if\ charging \\ -d_t^{\{r,i\}} & if\ discharging \end{cases} \quad 7.8$$

Net power injected/drawn from the grid by the k^{th} Charging Stations could be obtained using the (2.58).

$$P_k^{CS} = \sum_{i=1}^{nev} P_i^{EV} \quad 7.9$$

7.5.2 Modeling of DER

The Wind and Solar PV based $DERS$ have been modeled using the equivalent average models. The uncertainty modeling has been done using the beta distribution for solar-based DER and Weibull distribution for wind-based DERs. Many models have been proposed in the literature for short term load forecasting that may be utilized for forecasting the load of the impending hours. The predicted wind speed and solar irradiance have been used to obtain the equivalent power produced by the solar or wind DER using eq. (7.10) or (7.15).

$$f(s_i) = \begin{cases} \frac{\tau(\alpha_i + \beta_i)}{\tau(\alpha)\tau(\beta_i)} \cdot s_i^{\alpha_i - 1} \cdot (1 - s_i)^{\beta_i - 1} & for\ 0 \le s_i \le 1; \alpha \ge 0; \beta_i \le 0 \\ 0 & otherwise \end{cases} \quad 7.10$$

Where, $s_i \in [0,1]$ stands for the solar irradiance (kW/m^2), $f(s_i)$ represents the probability distribution factor (Beta), with s_i α_i and β_i as the parameters of beta pdf.

Table 7.2 $EVagent$ taxonomy.

$EVagent$	Field	Detail
	SoC	State of Charge
	t	Time
	V_{id}	Vehicle id
	loc	Location of the EV
	av	Availability of EV
	$Tstopa$	Estimated stopping time if vehicle is running
	$Tstarta$	Time at which the trip started
	$Prob$	Probability of connecting to grid for charging/discharging.
	$Dmax$	Maximum estimated distance that EV can travel based on current SoC
	D	Distance travelled in current trip.
	c_{stat}	Charging status
	Te	Time elapsed from the start of current ride.
	Tr	Estimated time remaining in current ride.
	$Speed$	Speed of the vehicle.
	Cs_d	Array vector containing the distance information from the nearest charging station.
	C_{db}	Array containing information of charging station accepting the request of allowing the vehicle to charge.
	CS_{name}	Charging station name/id
	C_r	Charging/discharging rate at which vehicle is feeding or absorbing power from-to grid
	Tcs	Time at which the vehicle is connected to the charging station

Table 7.3 Structure Field and their details for Charging Station (CS_{Agent}).

CS_{Agent}	Field	Detail
	Cap	Capacity of the CS
	Rem_{Cap}	Remaining capacity of the CS
	Av	Indicator for availability for charging from CS
	D_c	Number of connected devices
	Cc1	Rate of charging for type 1 charger
	Cc2	Rate of charging for type 2 charger

After modeling of solar irradiance, the solar plant output can be modeled as

$$P_i^s = g_s(s_i, \theta_i^s) = N_i \cdot FF_i \cdot V_{yi} \cdot I_{yi} \quad 7.11$$

$$I_{yi} = s_i \cdot [I_{sc_i} + k_{c_i}(T_{ci} - 25) \quad 7.12$$

$$V_{yi} = V_{oc_i} - k_{vi} \cdot T_{ci} \quad 7.13$$

$$T_{c_i} = T_{\alpha_i} + s_i \cdot \frac{N_{ot_i} - 20}{0.8} \quad 7.14$$

Where, P_i^s , $g_s(\cdot)$, θ_i^s, k_{vi}, k_{ci} are output power of the i^{th} the solar power plant, solar generation function, operational parameter, voltage, and current temperature coefficients. FF_i is the fill factor, I_{sc_i},V_{oc_i}, V_{MPP_i} represents the short circuit current (A), open-circuit voltage (V), and maximum power point voltage. The N_{oc_i}, T_{ci}, and $T_{\alpha i}$ are normal operating temperature, cell temperature, and ambient temperature, respectively. For the wind power plant, the uncertainty in wind speed has modeled using

$$F(v_i) = \frac{k_i}{c_i}\{\frac{v_i}{c_i}\}^{(k_i-1)} exp[-(\frac{v_i^{(k_i-1)}}{c_i})] \quad 7.15$$

$$P_i^w = g_w(v_i, \theta_i^w) = \begin{cases} 0 & \\ P_{ri} \cdot \dfrac{v_i - v_{ci}}{v_{ri} - v_{ci}} & v_{ci} \le v_i \le v_{ri} \\ P_{ri} & v_{ri} \le v_i \le v_{coi} \end{cases} \quad 7.16$$

Here, k_i, $v_i(\geq 0)$, and c_i are shape index, wind speed, and scale index, respectively. Whereas, θ_i^w, $v_c i$, v_{coi}, v_{ri} and P_{ri} are the operation parameter, cut-in, cut-out, and rated wind speed, and rated power output of i^{th} wind DG.

7.6 PROBLEM FORMULATION OF DSO

7.6.1 Loss Minimization

The information pertaining to the forecasted/estimated generation/load at each node of ADN would be acquired by the DSO. The DSO would determine the optimal control settings for meeting the desired operational objectives. In the proposed method, the DSO

aimed at minimizing the overall losses of the ADN. This has been achieved by minimizing the objective function given in equation

$$Min\left(\mathcal{L}(t) = \sum_{i=0}^{n-1} r_i \frac{P_{i,t}^2 + Q_{i,t}^2}{V_{i,t}^2}\right) \quad 7.17$$

In (17) $\mathcal{L}(t)$ is the total loss of the ADN at time t. $P_{i,t}$, $Q_{i,t}$ and $V_{i,t}$ are active power, reactive power and voltage at i^{th} bus respectively whereas r_i is the resistance between i^{th} and $i^{th} - 1$ bus, n is the total number of branches. The parameters to be controlled in the ADN includes the tap settings of OLTC, the number of the capacitor bank, and voltage regulators deployed in the distribution network. The objective of (17) is achieved by the DSO while adhering to the underlying equality and inequality constraints.

7.6.1.1 *Equality Constraints*

$$P^{source} + P^S + P^W \pm P^{CS} - P^{load} - P^{loss} = 0 \quad 7.18$$

Here, P^W and P^S represents the total wind and solar power fed into the ADN, P^{load} , P^{loss} are the total load, and total losses of the ADN while P^{CS} is the total power drawn by the charging stations. These values are expressed in the equations

$$P^S = \sum_{i=1}^{ns} P_i^s;\ P^W = \sum_{j=1}^{nw} P_j^W \quad 7.19$$

$$P^{CS} = \sum_{k=1}^{ncs} P_k^{CS};\ P^{load} = \sum_{m=1}^{nl} P_m^{load} \quad 7.20$$

$$P_{loss} = \sum_{i=0}^{n-1} r_i \frac{P_{i,t}^2 + Q_{i,t}^2}{V_{i,t}^2} \quad 7.21$$

7.6.1.2 *Inequality Constraints*

$$P_{i,j}^{min} \leq P_{i,j} \leq P_{i,j}^{max} \quad 7.22$$

$$Q_{i,}^{min} \leq Q_{i,j} \leq Q_{i,j}^{max} \quad 7.23$$

$$V_i^{min} \leq V_i \leq V_i^{max} \quad 7.24$$

7.6.2 ADC Evaluation

The ADC expressed by (7.4) could be defined as a maximization problem given as (7.25).

$$Max\lambda \quad 7.25$$

$$\text{where:} \quad \lambda = \sum_{i=1}^{nl} Pd_i - \sum_{i=1}^{nl} Pd_0 \quad 7.26$$

$$\text{s. to:} - P^{source,min} \leq P^{source} \leq P^{source,max} \quad 7.27$$

Along with the constraint mentioned in (7.27) the power flow constraints.

7.6.3 Blockchain Efficiency Factor (BC_{ef})

To assess the impact of energy trading over blockchain and its impact on the ADN a novel index BC_{ef} have been proposed in this article. The index BC_{ef} could be mathematically defined as

$$BC_{ef} = \frac{TEP}{TELMCP + TELMP} \quad 7.28$$

Where, TEP is the product Total Energy and Price for base case. TELMCP is the product of total energy sold at LMCP and LMCP when block chain based energy transaction is considered. TELMP is the product of total energy sold at LMP under block chain energy transaction.

When the block chain based energy transaction is simulated then following cases may be seen:-

a) LMCP < LMP

In this case the LMCP is considered for bid settlement till the localized market clearing volume. Beyond the LMCV the energy is sold at the LMP.

b) LMCP>LMP

In this case clearing price would be set as LMP and entire buying bid would be setteled at this price.

The factor BC_{ef} represents the extent to which the blockchain-based energy transaction affects the grid operation in terms of economies and losses. If the value is unity, then there is no effect of incorporating blockchain-based energy transactions.

7.6.4 Solution Methodology

Pattern Search (P.S) based optimization technique has been used for solving the objective functions expressed by (7.17) and (7.25). The application of PS for ATC assessment and enhancement at the transmission level has been investigated in [99]. Being a direct search algorithm, in PS, information pertaining to the objective function's gradient is not required. The direct search algorithm searches a set of points around the current point, looking for the problem's optimum point.

7.7 RESULT ANALYSIS AND DISCUSSION

The proposed method of this chapter has been utilized for testing on the modified IEEE 123 bus test system as inked in Figure 7.8. Modification to the test system has been done by incorporating

i. Public charging stations of 200 kW capacity at nodes 60 and 76.

ii. At nodes 35 and 29, two wind DER have 800 kW, and 700 kW rating have been placed.

iii. Nodes 26, 100, 65, and 54 are provided with PV DER having ratings of 400, 100, 400, and 400 each.

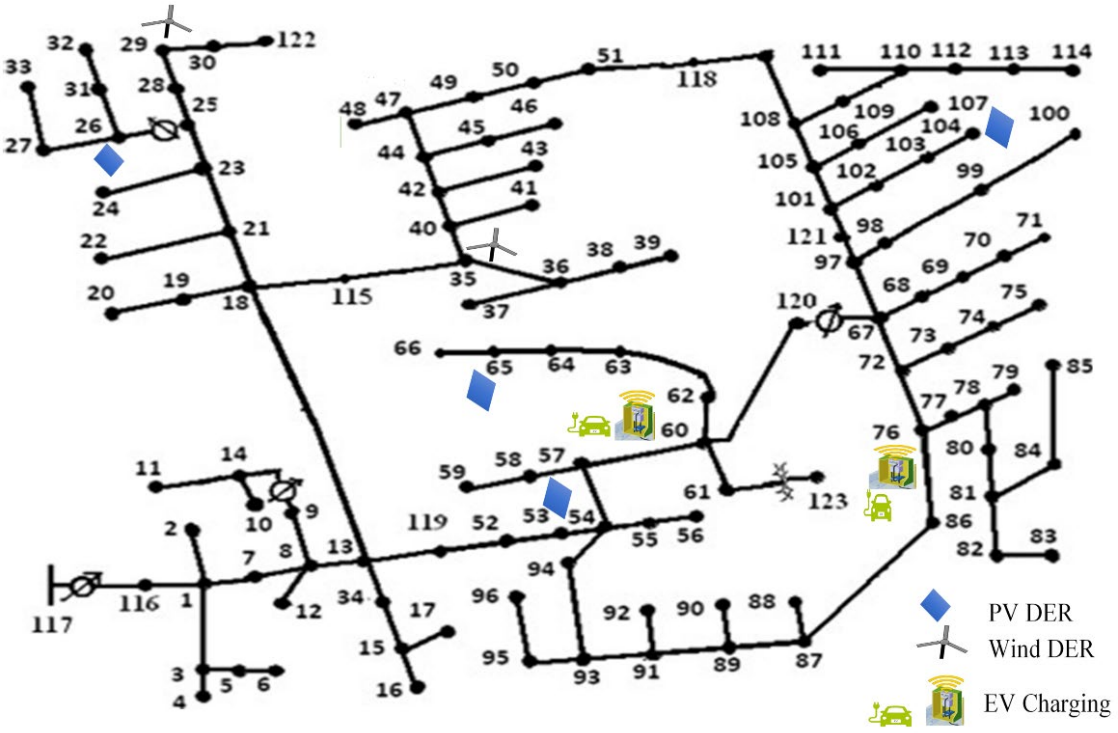

Figure 7.8 Test System: Modified IEEE 123 bus feeder.

Table 7.4 Various Cases considered for the analysis.

S.N	Component	Case 1	Case 2	Case 3	Case 4
1	PV	×	✓	✓	✓
2	WIND	×	✓	✓	✓
3	EV	×	×	✓	✓
4	MG	×	×	×	✓

The system has been analyzed for four different cases details of various cases could be found in Table 7.4. Namely, four different cases have been considered depending upon the consideration of PV, WIND, EV, and MG. For the base case, i.e., 'Case 1', the energy trading via blockchain has not been considered. In contrast, blockchain-based energy trading has been considered for all the other cases. The Load Margin plot for various cases of Modified IEEE 24 bus test system under study has been shown in Figure 7.9. The results are shown corresponding to all four cases at a resolution of 15 mins for the duration of 24 hrs. It can be observed that the LM depends on the time of day as well as the activeness of the various energy vendors in the market, and hence the blockchain-based energy transaction affects the LM of the overall system.

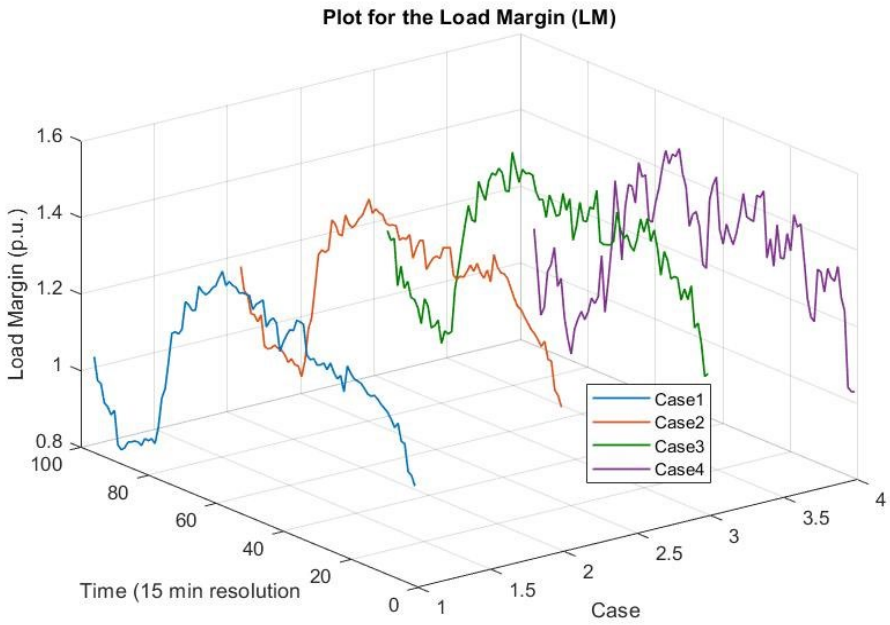

Figure 7.9 Load Margin plot for various cases of Modified IEEE 24 bus test system

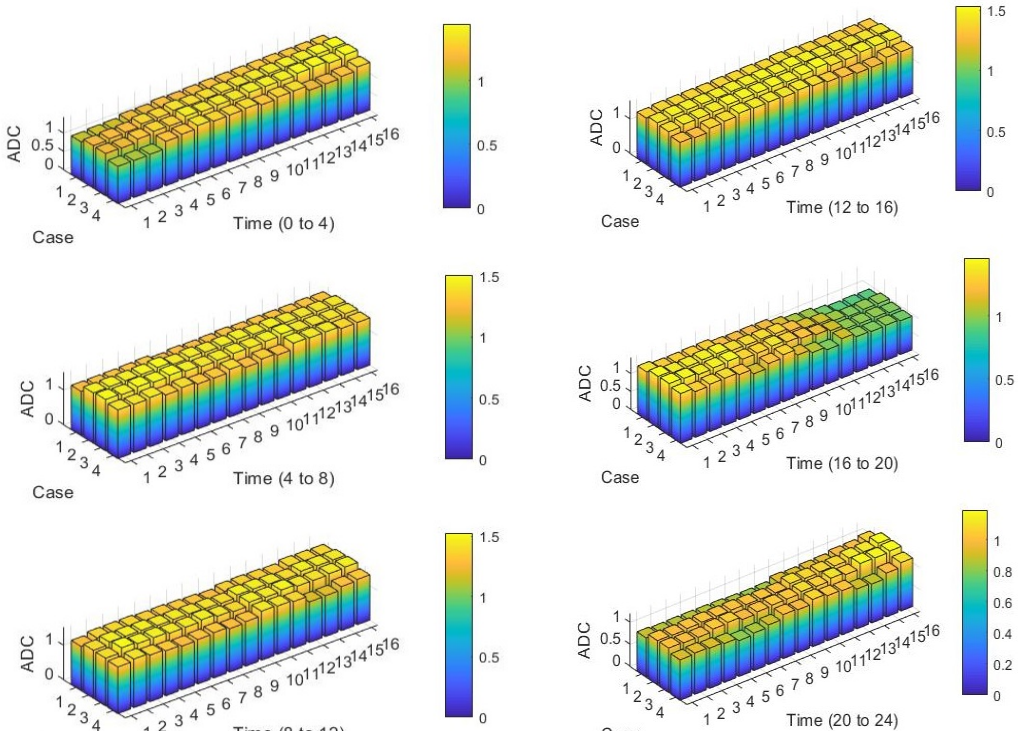

Figure 7.10 ADC of ADN at resolution of 15 min for 24 hrs.

The ADC variation for the considered test system has been shown in Figure 7.10. The result has been shown in terms of bar plot, and each subplot contains the plot for 4 hours duration. It can be observed from the figure that the ADC of the ADN depends on the time of the day. It is also seen that considering Block-chain based energy transactions affects the ADC of the system. The ADC information would be vital in the techno-economic operation of ADN when multiple, and probably mobile source/sink of electric power (i.e., EV) are being integrated more and more into the ADN grid. The ADN's aggregated load at the interface of transmission and distribution system also gets affected on account considering the presence of DERS and energy trading through the block-chain-based mechanism, that can be inferred from the various subplots shown the Figure 7.11.

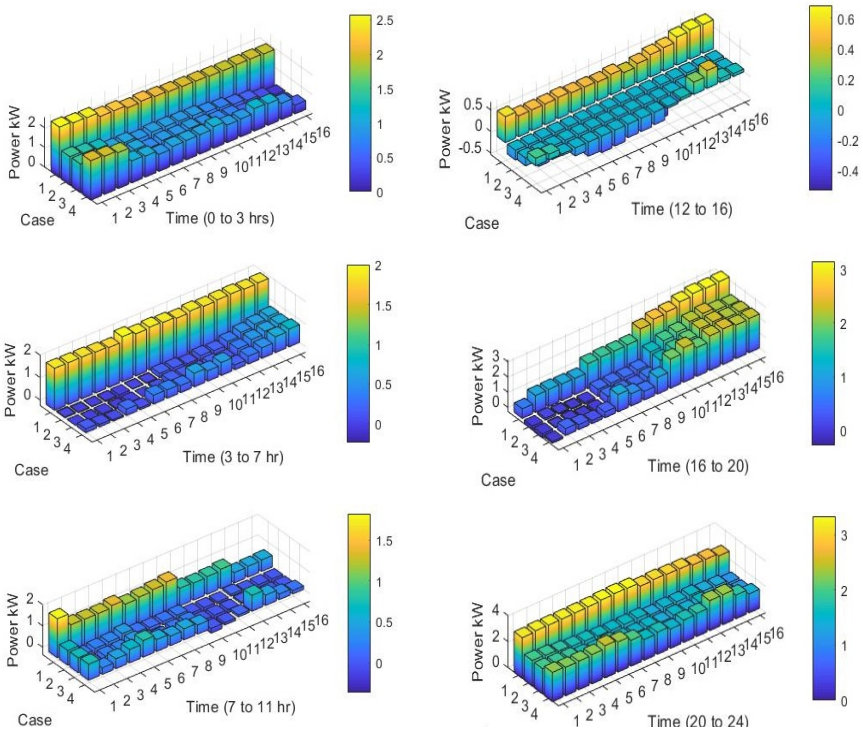

Figure 7.11 Aggregated Load Profile of ADN at resolution of 15 min for 24 hrs.

It can be observed from the subplot for time duration 12 to 16 p.m. that at some time instants the ALP is negative. These instants represent the scenario for which the total generation of the ADN surpasses its load and feeds power back to the grid. The LMCP determination for the considered test system has been shown for a typical case in Figure 7.12. Here the intersection points of sellers and buyers bid amount are taken as the LMCP. In the plot, the LMCP value is 3.8, and LMCV (localized marginal clearing volume) is 1800 kW. Further, in Figure 7.13, the market-clearing price of ADN under various cases is shown. The plot for case 1 (i.e., base case) represents LMP (locational marginal cost) subtended at the DSS for the considered test system.

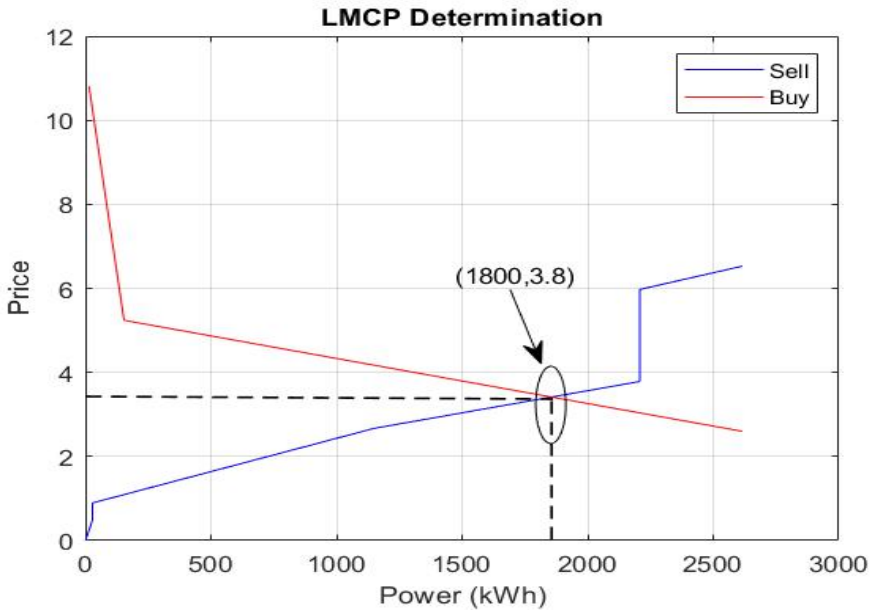

Figure 7.12 Illustration of LMCP determination.

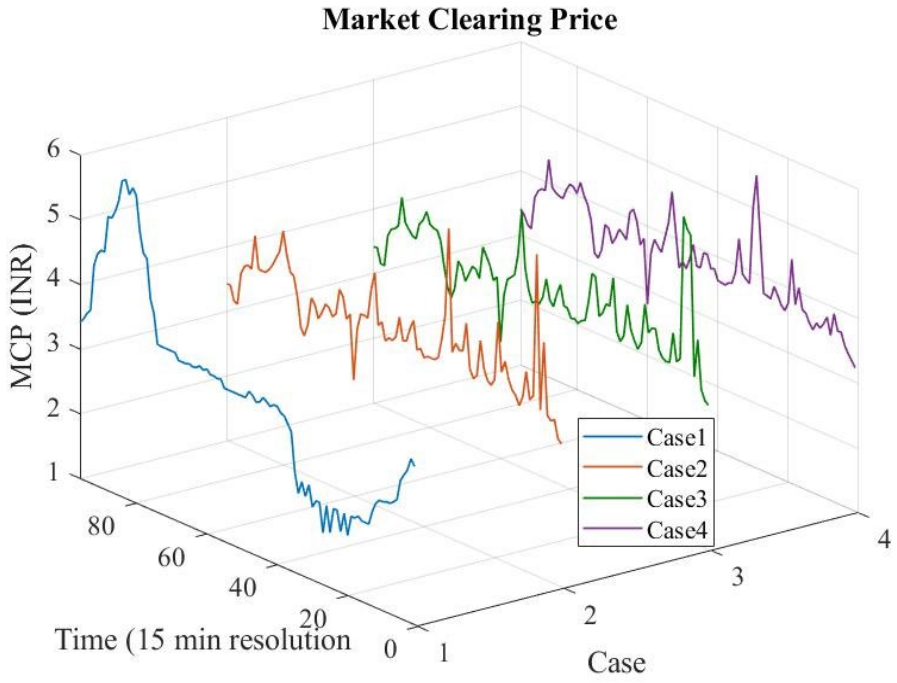

Figure 7.13 LMCP of ADN at a resolution of 15 min for 24 hrs.

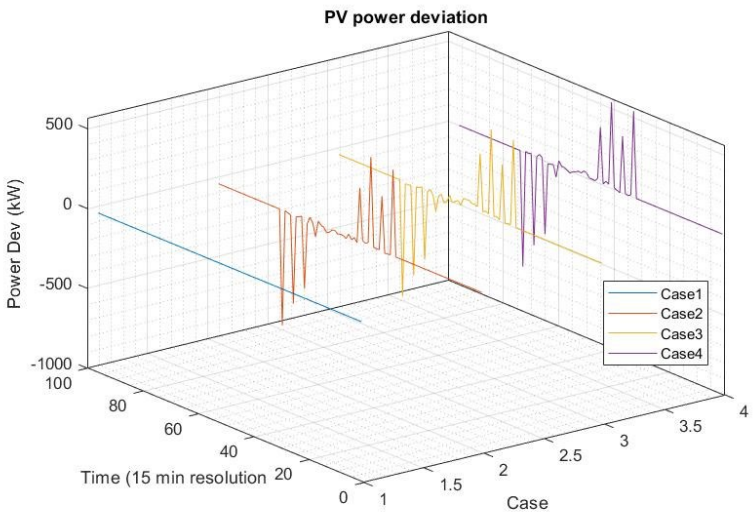

Figure 7.14 PV power deviation of ADN at a resolution of 15 min for 24 hrs.

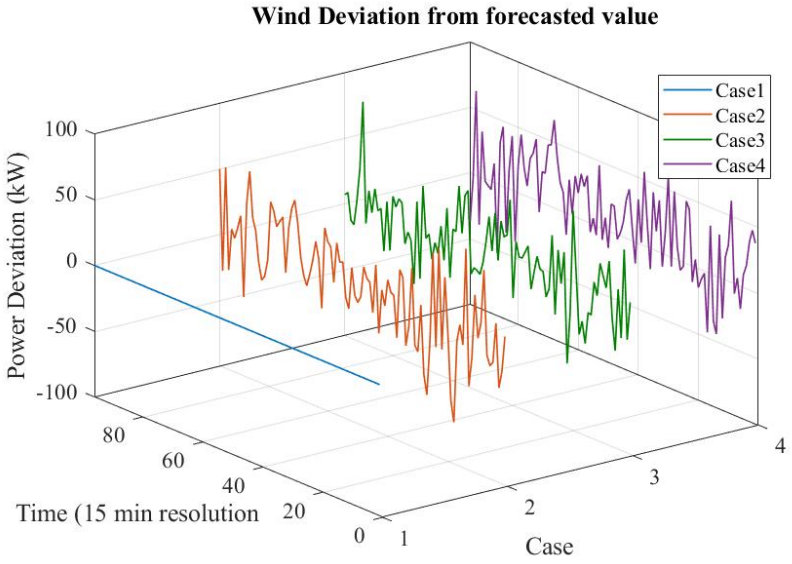

Figure 7.15 Wind power deviation of ADN at resolution of 15 min for 24 hrs.

The market data of Gujrat (practical Indian data) have been considered for the analysis purpose. The LMCP determined with the method proposed in this article has been drawn for the other three cases. The deviations in power for PV DER and Wind DER have been shown through the plots of Figure 7.14 and Figure 7.15.

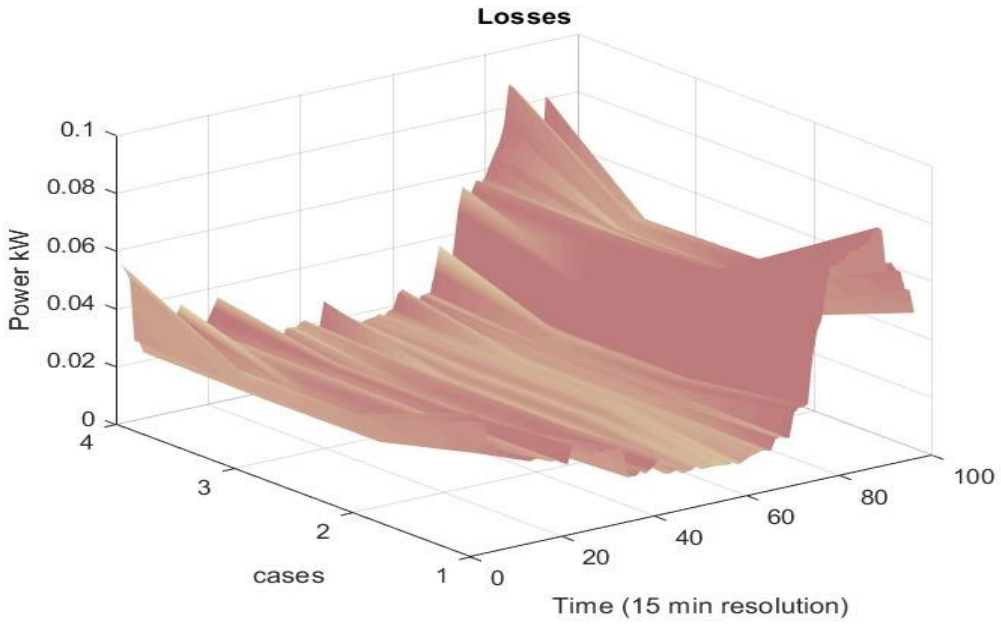

Figure 7.16 Losses of ADN at a resolution of 15 min for 24 hrs.

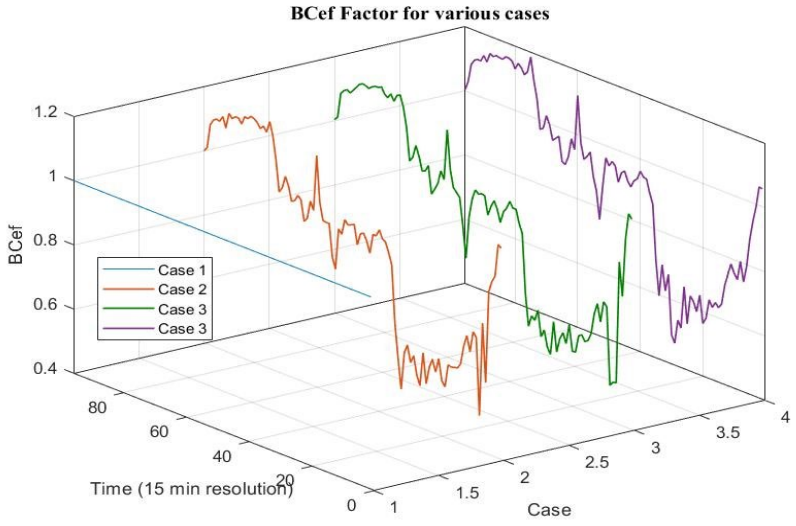

Figure 7.17 BC_{ef} factor of ADN at resolution of 15 min for 24 hrs.

These deviations represent the difference between the forecasted and actual power at a particular time instant. These plots are significant as these highlights the uncertainty and degree of variability is introduced into the grid from the ADN. The value of deviations for Case1 (i.e., base case) is zero at all the time instants because PV and $Wind\ DERS$ are not considered in the base case. The comparative visualization of losses for all the cases has also been illustrated through the plot of Figure 7.16. It can be inferred that the losses,

although depends on the time of day, reduces when the load is locally supplied by the DERs, which are actively participating in blockchain-based energy transaction. The blockchain efficiency factor proposed in this chapter have been obtained for each instant and plotted in Figure 7.17. It could be observed from the BC_{ef} for case 1 is 1, as block-chain based energy transaction have not been considered during the base case simulation. The factor BC_{ef} as seen from the plot for other cases can vary from one-time instant to another time instant; the effect of blockchain becomes more and more dominant when the number of active devices in the system increase.

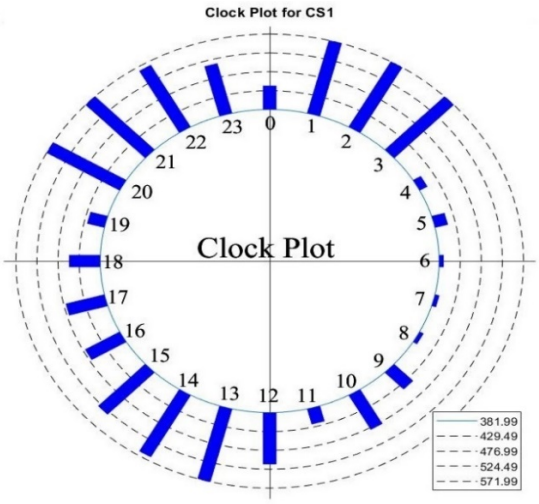

Figure 7.18 Clock plot showing the CS1 power demand over 24 hrs.

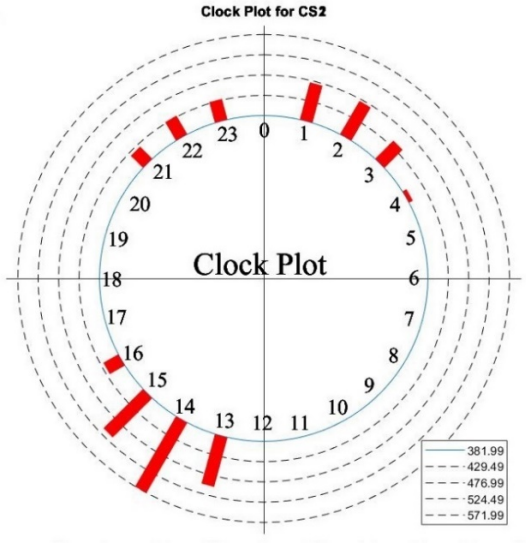

Figure 7.19 Clock plot showing the CS2 power demand over 24 hrs.

Table 7.5 Bid and actual value of Power (kW) and Price (INR/kW).

SN	Component	Time				Time			
		10:00 AM				12:00 PM			
		Bid		Actual		Bid		Actual	
		Power	Price	Power	Price	Power	Price	Power	Price
1	PV 1	48.3682	5.9	47.3513	3.63	97.222	5.96	95.2177	3.77
2	PV 2	191.348	5.974	189.4047	3.63	387.9903	5.974	380.8725	3.77
3	PV 3	193.8066	5.89	189.4043	3.63	384.5391	5.9152	380.8744	3.77
4	PV 4	468.6877	2.44	466.2471	3.63	923.7549	2.51	929.1471	3.77
2	WIND 1	834.6963	3.784	816.0642	3.63	558.073	3.784	540.9797	3.77
3	WIND 2	342.2129	6.15	327.3964	3.63	223.3798	6.3	219.8758	3.77
3	EV	170.254	4.8595	170	3.63	147.4016	5.1332	150	3.77
4	MG	33.2089	7.052	30	3.63	59.4385	7.167	60	3.77

Higher the deviation of BC_{ef} from unity, higher would be the impact of considering the blockchain-based energy transaction on ADN. The clock plots of Figure 7.18 and Figure 7.19 have been used to show the net load subtended by the EVCS to the grid. It can be observed that the power drawn from the grid would depend on the time of day. It is imperative to mention that the effect of incorporation of the EV would become more dominant if the number of $EV's$ used in the simulation process are increased. The bid and actual values of various components of ADN have been inked in Table 7.5. In this table,

the bid value of the component is the bid submitted at $(t-1)^{th}$ instant (t being the current instant). The actual value is the actual power sold or purchased to/from the grid. The actual price represents the LMCP determined at and used for clearing/settling the transactions. The actual power withdrawal/injected by each peer is communicated to the blockchain at the smart contract address. Through smart contracts, the financial settlements could be materialized without the necessity of third party mediation.

7.8 CONCLUSION

The effect of distributed energy resources and their participation in energy trading over a blockchain-based framework has been analyzed. The impact has been investigated primarily on the available distribution capability, aggregated load profile, and load-ability limit of the active distribution network. The concept of localized market clearing price and localized market clearing volume has been introduced, and the methodology for its determination is discussed. An index BC_{ef} for quantifying the impact of blockchain-based energy trading has been proposed. The technique presented has been applied to the modified IEEE 123 bus distribution system. It could be inferred from the results obtained during the simulations that employing blockchain for energy transactions would have a considerable effect on ALP, ADC , LM, and losses of the ADN. Thus, if appropriately utilized, the blockchain-based system could help in efficiently managing both economic and operational aspects of the ADN.